

Effect of tungsten dissolution on the mechanical properties of Ti–W composites

Heeman Choe^a, Susan M. Abkowitz^b, Stanley Abkowitz^b, David C. Dunand^{a,*}

^a Department of Materials Science and Engineering, Northwestern University, Evanston, IL 60208, USA

^b Dynamet Technology Inc., Eight A Street, Burlington, MA 01803, USA

Received 28 June 2004; accepted 2 August 2004

Abstract

Blends of 90 wt.% Ti and 10 wt.% W powders were consolidated by powder metallurgy, using an initial W powder size that was very fine (0.7 and 2 μm) or very coarse (<250 μm). Dissolution of W powders in the Ti matrix during consolidation was almost complete for the former blends (thus forming Ti–10W “alloys”) but very limited for the latter blend (thus forming a Ti–10W “composite”). The Ti–10W alloys exhibit much higher yield and tensile strengths than the Ti–10W composite, indicating that tungsten strengthens titanium more efficiently as a solute atom (solid-solution strengthening) than as a second phase (composite strengthening by load transfer). The Ti–10W alloys also exhibit much higher ductility than the Ti–10W composite, whose brittle W particles exhibit fracture or pull-out from the matrix.

© 2004 Elsevier B.V. All rights reserved.

Keywords: Composite materials; Dental alloys; Powder metallurgy; Mechanical properties; Metallography

1. Introduction

Titanium and its alloys, originally developed as aeronautical materials, are used as bone-replacement implants due to their bio-compatibility, low density, static and fatigue strength, corrosion resistance, and lack of magnetism (important for magnetic resonance imaging after implantation) [1,2]. Another critical requirement for implants is wear resistance, as wear debris can cause severe inflammatory responses in surrounding tissue [1,2]. However, the wear resistance and strength of commercially pure titanium (CP-Ti) is relatively poor, which makes it insufficient for highly stressed bone implants or wear-prone prostheses [3]. A solution to both strength and wear-resistance limitations is to add to titanium a hard ceramic reinforcement that is thermodynamically stable with the matrix, e.g. titanium carbide or boride. The resulting metal matrix composites however exhibit low ductility and toughness [4]. Recently, it has been shown that tungsten particles can be added to a titanium matrix,

resulting in a Ti–W composites with outstanding strength and hardness (which generally scales with wear-resistance), and only a minor ductility penalty [5]. Moreover, tungsten is non-magnetic and, in solid solution, is known to decrease the elastic modulus of titanium [5], which helps alleviate stress-shielding arising from differences in compliance between the implant and the host tissue [1]. Unlike ceramic reinforcement, tungsten has unlimited solubility in titanium at the composite densification temperature. For short processing times when partial dissolution of the W particles occurs, the composite then consists of a Ti–W matrix containing partially dissolved W particles, as shown in a previous study [5]. In that study, however, the relative importance of solid-solution strengthening and composite strengthening was not investigated.

Here, we present a study of the microstructure and mechanical properties for a series of Ti–10 wt.% W alloys produced by powder metallurgy using W powders with size varying over a wide range. This allows to vary the degree of W dissolution from small to nearly complete, and to probe the relative importance of solid-solution strengthening and composite strengthening for tungsten in titanium.

* Corresponding author. Tel.: +1 847 491 5370; fax: +1 847 467 6573.
E-mail address: dunand@northwestern.edu (D.C. Dunand).

2. Materials and methods

Three Ti–10 wt.% W blends were mixed using different W powder size. The W powder sizes spanned two orders of magnitude: 0.72 μm (for Alloy 1), 2 μm (for Alloy 2), and <250 μm (for Alloy 3), as summarized in Table 1.

Processing was by the combined cold and hot isostatic pressing (CHIP) technology [6] as follows. A blend of Ti powders (<150 μm) and W powders were compacted into green billets by cold-isotatic pressing at a pressure of 379 MPa. The billets were then vacuumed-sintered at 1230 $^{\circ}\text{C}$ for 4 h and densified by hot-isostatic pressing (HIP) at 900 $^{\circ}\text{C}$ for 2 h at 100 MPa [5], followed by slow cooling within the press. Billet density was, within experimental error, equal to the theoretical value of 4.9 g/cm³, indicating that complete densification had been achieved.

The microstructure of the Ti–W alloys was evaluated by optical microscopy on cross-sections produced by grinding on SiC paper, polishing with diamond and alumina slurries, and etching with a modified Kroll's reagent (5% nitric acid, 10% HF, and 85% water). Chemical composition profiles were achieved by energy-dispersive spectroscopy (EDS, Hitachi S-3500) with a spot size of 15 nm. Matrix micro-hardness was measured with a Vickers indenter using a 100–200 g load and an indent time of 10 s on epoxy-mounted cross-sections in matrix regions far from W particles.

Tensile tests were performed at ambient temperature on one specimen of each alloy, machined to ASTM E-8 proportional standards with 36 mm gauge length and 6.4 mm gauge diameter. The cross-head speed was 12.7 mm/min, corresponding to an initial strain rate of $6.2 \times 10^{-3} \text{ s}^{-1}$. The strain was measured with an extensometer with 25.4 mm gauge length. Fracture surfaces were examined in a scanning electron microscope (SEM).

3. Results

Fig. 1(a)–(c) shows micrographs of etched cross-sections for Alloys 1–3, which exhibit the following features: (i) white particles; (ii) a surrounding dark-etched shell, ca. 50 μm thick; (iii) an etched acicular matrix. These features were identified previously [5] as: (i) partially dissolved W particle; (ii) matrix diffusion zone with high W content; (iii) matrix

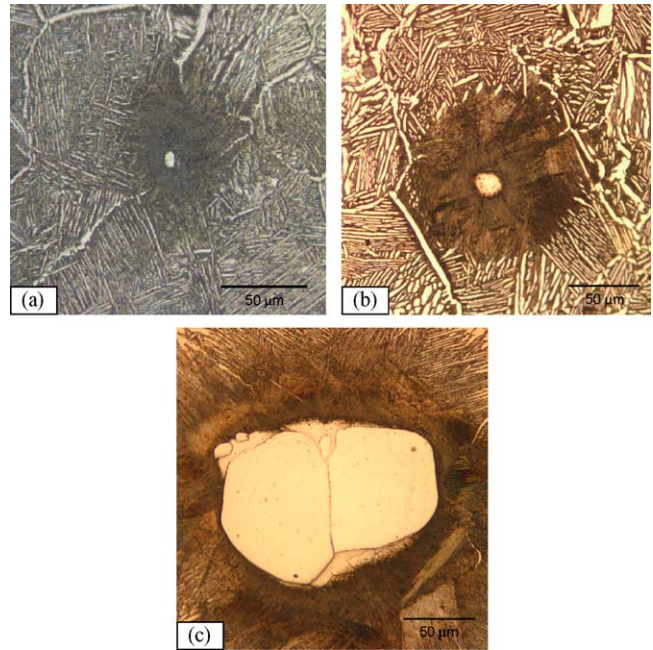


Fig. 1. Optical micrographs of Ti–10W alloys showing a W particle, an adjacent dark-etched matrix shell with high W content and the surrounding α/β etched matrix (a) Alloy 1 with 0.7 μm initial W powder average size and 0.006 vol.% W particles; (b) Alloy 2, with 2 μm initial W powder average size and 0.07 vol.% W particles; (c) Alloy 3 with <250 μm initial W powder average size and 2.25 vol.% W particles, showing a W particle cluster.

with Widmanstätten α/β structure with most of the W segregated in the β phase. Alloys 1 and 2 with micron-size initial W powder exhibit almost no remaining un-dissolved W particles, while many such particles are visible in Alloy 3 with much coarser initial powders. In Alloys 1 and 2, the few remaining W particles are equiaxed, uniformly distributed and 10–20 μm in size (Fig. 1a and b). In Alloy 3, the particles are much larger (119 μm average size, Table 1), tend to be more irregular in shape and can be clustered (Fig. 1c). Table 1 summarizes the W particle size and volume fraction, as well as the calculated average matrix W content.

EDS composition profiles are shown in Fig. 2 for Alloys 1 and 3, measured from the center of a W particle into the matrix. The W content decreases monotonously from 96 (at particle center) to 10 wt.% W (in matrix) over a distance of $\sim 90 \mu\text{m}$ for Alloy 1. A similar gradient is observed for Alloy

Table 1
Tungsten powder and particle parameters in Ti–10W Alloys

Alloy	W powder type	Average size of initial W powders (μm)	Size of W particles (μm) in composite ^a	Volume fraction of W particles in composite (%)	Extent of W powder dissolution in composite (%)	Matrix average W concentration in composite ^b (wt.%)
1	FSSS ^c 0.72	0.7	11 \pm 8	0.006	99.8	9.98
2	FSSS ^c 2.02	2	20 \pm 8	0.07	97	9.74
3	–60 mesh	<250	119 \pm 54	2.25	10	1.23

^a Apparent size in metallographic sections with error given as standard deviation.

^b Calculated from measured W particle volume fraction assuming an overall W content of 10 wt.%.

^c Fisher sub-sieve size.

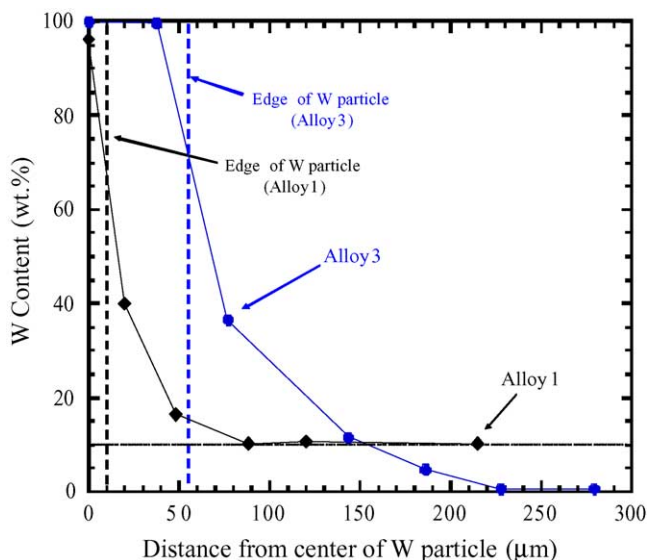


Fig. 2. EDS composition profiles from the center of an arbitrarily selected W particle into the Ti matrix for Alloy 1 (with most W dissolved) and Alloy 3 (with most W un-dissolved).

3, but the matrix composition is ~ 0 wt.% W at a distance of ~ 170 μm from the particle edge (Fig. 2). The hardness profile measured for the same Alloys 1 and 3 (Fig. 3) shows that particles are much harder than the matrix, whose hardness reaches a minimum in the diffusion zone adjacent to the particles, before achieving values of ca. 400 and 300 HV for Alloys 1 and 3, respectively, in good agreement with average matrix values listed in Table 2.

Fig. 4 shows the tensile stress–strain curves for the three Ti–10W alloys together with that of pure CP-Ti fabricated by the same processing route [5]. The corresponding mechanical properties are listed in Table 2, and also included

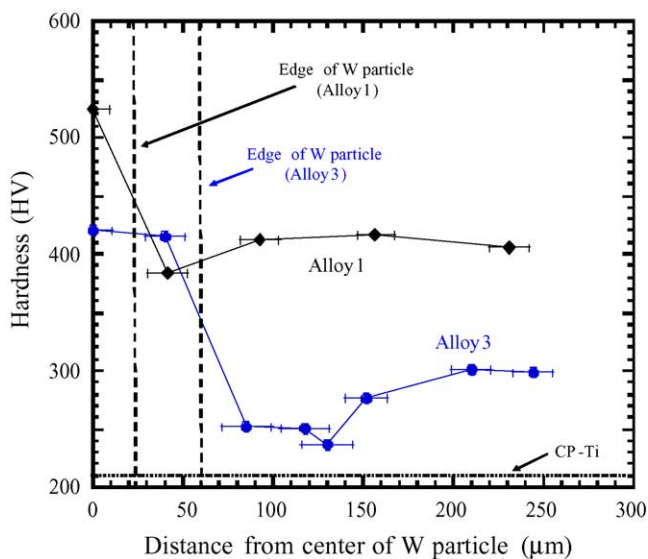


Fig. 3. Microhardness profiles from the center of a randomly selected W particle into the Ti matrix for Alloy 1 (with most W dissolved) and Alloy 3 (with most W un-dissolved).

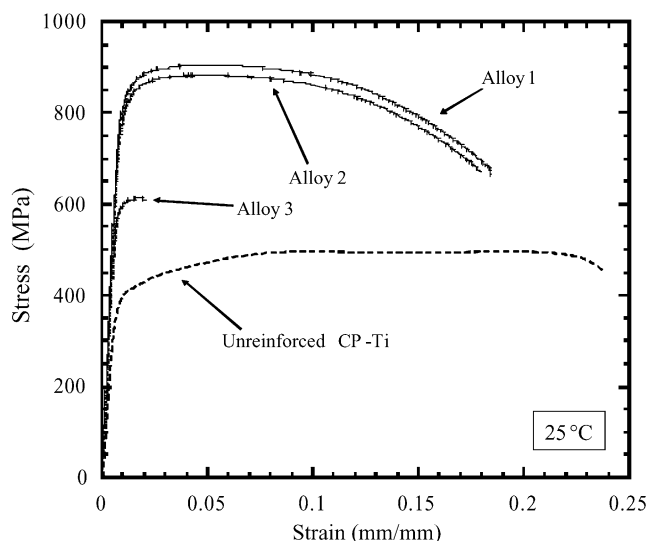


Fig. 4. Tensile stress–strain curves of Ti–10W alloys: Alloys 1 and 2 (with most W dissolved) and Alloy 3 (with most W un-dissolved). Also shown for comparison is the curve for W-free CP-Ti produced by the same powder-metallurgy route [5].

for comparison is a Ti–10W alloy produced from 3 μm W powders [5]. Alloys 1 and 2, with almost all the W in solid-solution, have nearly overlapping stress–strain curves which show very high yield and ultimate strengths as compared to CP-Ti. These alloys also show considerable necking, with ductility values that are only somewhat lower than that of CP-Ti. On the other hand, Alloy 3, with large W particles, fractured shortly after reaching its ultimate tensile strength (UTS) which, together with its yield strength, is closer to that of CP-Ti than those of Alloys 1–2. Table 2 also shows that good agreement exist between the mechanical properties of Alloy 2 (made with 2 μm W powders) and those of a previously studied Ti–10W alloy produced from 3 μm W powders [5].

SEM pictures of fracture surfaces for Alloys 1 and 3 are shown in Fig. 5. The stronger and more ductile Alloy 1 is characterized by pockets of spherical dimples in the matrix (Fig. 5a). For Alloy 3, matrix dimples are larger than for Alloy 1 (Fig. 5c), and fractured W particles are observed (Fig. 5d), together with particle pull-out (Fig. 5b).

4. Discussion

4.1. Microstructure

The equilibrium Ti–W phase diagram is characterized by a eutectoid reaction at 740 $^{\circ}\text{C}$ where a Ti–W solid solution decomposes into Ti-rich and W-rich phases, without any intermediate intermetallic phases [7]. Above 882 $^{\circ}\text{C}$, there is complete solubility between Ti and W, so that the sintering and HIP steps at 1230 and 900 $^{\circ}\text{C}$ are expected to promote complete dissolution of the W powders. The W particle vol-

Table 2
Tensile properties and matrix micro-hardness values of Ti-10W Alloys

Alloys	0.2% Yield stress (MPa)	Ultimate tensile strength (MPa)	Strain at UTS (%)	Failure strain (%)	Elastic modulus (GPa)	Matrix hardness (HV)
1	803	905	4.8	18.5	108	438 ± 10
2	784	884	4.7	17.9	101	420 ± 21
3	576	613	1.7	2.1	99	265 ± 21
Ti-10W [5]	769	931	5	14.1	110	300 ± 12
CP-Ti [5]	411	518	13	23.9	115	210 ± 20

ume fractions listed in Table 1 indicate that dissolution was almost complete (99.8 and 97%) for Alloys 1 and 2 with the fine 0.7–2 μm powders, but very limited (10%) for Alloy 3 with the coarsest powders. The latter alloy thus exhibits a non-equilibrium structure, consisting of a matrix with α/β Widmanstätten structure (typical of Ti alloys slowly cooled from the β -phase field [8]) and 2.25 vol.% W particles containing some Ti in solid solution. Also expected from diffusion kinetics is the smaller average size of the remaining W particles in Alloys 1 and 2 (Table 1). Furthermore, when observed by SEM, it is apparent that these particles consist of agglomerates of fine, micron-size W particulates, as also reported for a Ti-10W alloy processed from 3 μm W powders by the same route [5].

Fig. 2 shows that both Alloys 1 and 3 exhibit typical diffusion profiles away from the W particles, with W concentration reaching a steady state value of 10 wt.% at a distance of 80 μm from the interface for Alloy 1, and 0 wt.% at 170 μm from the interface for Alloy 3.

In Fig. 3, the hardness of the coarse W particle in Alloy 3 is in agreement with the range reported for pure W (350–445 HV [9]). The hardness of the fine W particle in Alloy 1 is however significantly higher (525 HV), which may be due to hardening by Ti in solid solution following diffu-

sion, and/or to the complex structure of the fine agglomerates forming those particles. The hardness profile show values at large distances from the particles that are in agreement with average matrix values given in Table 2, as expected. For both Alloys 1 and 3, however, hardness reaches a minimum in the diffusion zone where its W content is higher than matrix regions away from the W particles (Fig. 2). This unexpected result is probably due to the formation of complex metastable phases whose structure (and thus probably hardness) change with W content. In binary Ti-W alloys, hexagonal martensite (α') is formed below ~ 8 wt.% W, orthorhombic martensite (α'') exists between ~ 8 and ~ 24 wt.% W, beyond which orthogonal ω precipitates can form. Additionally, the formation of the metastable phases is further complicated by their quenching and aging history [7,10,11].

4.2. Strength and hardness

Two mechanisms may contribute to the increase in yield strength of the Ti-10W alloys as compared to CP-Ti: (i) solid solution strengthening of Ti by W, which is influenced by the W content of the matrix (both average and local); (ii) composite strengthening by the W particles, which is affected by their volume fraction, size and shape. Direct composite strengthening by load transfer is expected to be negligible, given the low volume fraction and equiaxed shape of the particles: Eshelby calculations based on elastic load transfer to spherical particles [12] predict an increase in yield stress with respect to CP-Ti by 6 MPa for Alloy 3 with the highest un-dissolved W volume fraction. Indirect composite strengthening by thermal-mismatch dislocations and grain size refinement is similarly negligible given the low volume fraction and relatively large size of the W particles. Finally, W particles are much too large for any significant dispersion strengthening. We thus conclude that the large differences in yield strength between Alloys 1–2 and Alloy 3 is due to differing extent in solid-solution strengthening. For Alloys 1 and 2 with the smallest initial W powders, the matrix composition is uniform, except in the immediate vicinity of the very few remaining W particles (Fig. 2). By contrast, for Alloy 3 with only one-tenth of its W content in solid solution, the matrix W composition drops to near zero at a distance of 175 μm from the particle edge (Fig. 2). Yielding is then controlled by the W-poor matrix regions between the W particles and their associated W-rich matrix regions. The volume fraction of W-poor region is estimated as 30 vol.%, calculated by con-

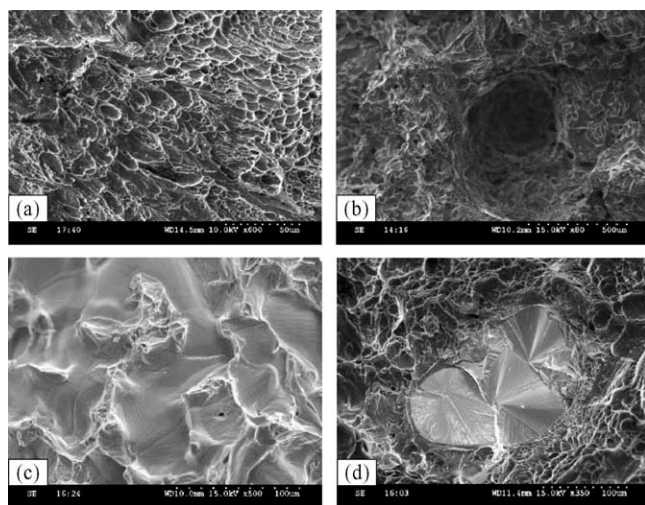


Fig. 5. SEM micrographs of the tensile fracture surfaces showing (a) pockets of dimples in the matrix of Alloy 1, typical of ductile failure; (b) a large depression due to W particle pull-out from the matrix in Alloy 3; (c) relatively large matrix dimples in Alloy 3; (d) brittle fracture of W particle cluster in Alloy 3.

sidering a W content of 5 wt.% at a distance of 190 μm from the particle center (Fig. 2) and an average particle radius of 60 μm (Table 1).

The average matrix hardness of Alloys 1 and 2 (ca. 430 HV) is exceptionally high: it exceeds the hardness of pure annealed W (350 HV [9]) and is close to that of work-hardened W (445 HV [9]), thus indicating that Ti–10W alloys are very wear-resistant. The hardness of Alloys 1 and 2 is higher than that reported previously for a Ti–10W alloy (300 HV [5]) which however used different W powder size (3 μm) and cooling rate after HIP, the latter being known to affect the non-equilibrium phases in the Ti–W system. Depending on composition and cooling process, it is possible to obtain a martensitic structure leading to a range of non-equilibrium phases, namely, α' , α'' , and ω with a concomitant change in mechanical properties [5,7,11]. By contrast, Alloy 3 is expected to be less wear-resistant due to its lower matrix average hardness and strength; in particular, W particle pull-out may become an issue for biomedical implant applications.

4.3. Ductility

The three Ti–10W alloys have very different ductilities: Alloys 1 and 2 exhibit large strain to failure (ca. 18%) and extensive necking, while Alloy 3 fractured shortly after reaching its UTS. This difference can be explained by the different volume fractions of hard and brittle W particles which can trigger early fracture. For the highly ductile Alloy 1, it is apparent that the inherent ductility of the Ti–10W matrix (as illustrated by the fine dimples typical of ductile tensile fracture, Fig. 5a) controls the fracture behavior, despite the occasional presence of W particles (Table 1). The low ductility of Alloy 3 is then not due to the limited ductility of its matrix but to the presence of the large, brittle W particles. Indeed, Alloy 3 shows evidence of both particle fracture and pull-out (Fig. 5d and b), indicative of particle cracking and reinforcement/matrix debonding, respectively, which are known in metal matrix composites to lead to a relatively brittle fracture behavior [13]. The clustering and relatively large size of W particles in Alloy 3 (Fig. 1c) are further reasons for its low ductility, as observed in other metal matrix composites [14–16]. In particular, the simulation work by Segurado et al. [17] shows that a small degree of particle clustering causes the fraction of broken particles to increase dramatically, leading to a large decrease in the overall composite flow stress and ductility.

5. Conclusions

- Blends of Ti–10 wt.% W powders were densified by powder metallurgy using W powders from very small

(0.7–2 μm) to very large (<250 μm) sizes. After processing, almost all the W is dissolved within the Ti matrix for the former materials, which are thus solid-solution “alloys” with a transformed α/β microstructure at ambient temperature. By contrast, for the latter materials, most of the W remains un-dissolved in the form of large metallic particles, resulting in a particulate-reinforced “composite”.

- The strength of the Ti–10W alloys is much higher than that of the Ti–10W composite, indicating that W is more efficient as a solid-solution strengthener than as a particle strengthener.
- The hardness of the Ti–10W alloys is higher and more uniform than that of the Ti–10W composite, and achieves values of ~ 400 HV, indicative of excellent wear resistance.
- The Ti–10W alloys are also much more ductile than the Ti–10W composite, which suffers from particle pull-out and fracture.

Acknowledgements

This research was supported by NIH through a SBIR grant to Dynamet Technology Inc. (Grant No. 2R44EB001005-02).

References

- [1] J. Black, *Biological Performance of Materials: Fundamentals of Biocompatibility*, 3rd ed., Marcel Dekker, New York, 1999.
- [2] F.H. Silver, D.L. Christiansen, *Biomaterials Science and Biocompatibility*, Springer-Verlag, New York, 1999.
- [3] D. Iijima, T. Yoneyama, H. Doi, H. Hamanaka, N. Kurosaki, *Biomaterial* 24 (2003) 1519.
- [4] M. Hagiwara, N. Arimoto, S. Emura, Y. Kawabe, H.G. Suzuki, *Iron Steel Inst. Jpn. Int.* 32 (1992) 909.
- [5] M. Frary, S. Abkowitz, S.M. Abkowitz, D.C. Dunand, *Mater. Sci. Eng. A* 344 (2003) 103.
- [6] S. Abkowitz, P.F. Weihrauch, S.M. Abkowitz, *Ind. Heat* 12 (1993) 32.
- [7] *Phase Diagrams of Binary Titanium Alloys*, American Society for Metals, Metals Park, OH, 1987.
- [8] *Materials Properties Handbook: Titanium Alloys*, American Society for Metals, Metals Park, OH, 1994.
- [9] *Metals Handbook: Properties and Selection: Nonferrous Alloys and Pure Metals*, American Society for Metals, Metals Park, OH, 1979.
- [10] E.W. Collings, *The Physical Metallurgy of Titanium Alloys*, American Society for Metals, Metals Park, OH, 1984.
- [11] J.C. Williams, B.S. Hickman, *Metall. Trans.* 1 (1970) 2648.
- [12] D. Hull, T.W. Clyne, *An Introduction to Composite Materials*, 2nd ed., Cambridge University Press, New York, 1996.
- [13] A. Miserez, A. Rossoll, A. Mortensen, *Acta Mater.* 52 (2004) 1337.
- [14] S.J. Hong, H.M. Kim, D. Huh, C. Suryanarayana, B.S. Chun, *Mater. Sci. Eng. A* 347 (2003) 198.
- [15] S. Seshan, M. Jayamathy, S.V. Kailas, T.S. Srivatsan, *Mater. Sci. Eng. A* 363 (2003) 345.
- [16] T.S. Srivatsan, M. Al-Hajri, C. Smith, M. Petraroli, *Mater. Sci. Eng. A* 346 (2003) 91.
- [17] J. Segurado, C. González, J. LLorca, *Acta Mater.* 51 (2003) 2355.